Lab on a Chip

PAPER

View Article Online
View Journal | View Issue

Cite this: *Lab Chip*, 2015, **15**, 1145

A high-power ultrasonic microreactor and its application in gas–liquid mass transfer intensification†

Zhengya Dong,[ab] Chaoqun Yao,[ab] Xiaoli Zhang,[c] Jie Xu,[c] Guangwen Chen,*[a] Yuchao Zhao[a] and Quan Yuan[a]

Received 6th December 2014,
Accepted 15th December 2014

DOI: 10.1039/c4lc01431f

www.rsc.org/loc

The combination of ultrasound and microreactor is an emerging and promising area, but the report of designing high-power ultrasonic microreactor (USMR) is still limited. This work presents a robust, high-power and highly efficient USMR by directly coupling a microreactor plate with a Langevin-type transducer. The USMR is designed as a longitudinal half wavelength resonator, for which the antinode plane of the highest sound intensity is located at the microreactor. According to one dimension design theory, numerical simulation and impedance analysis, a USMR with a maximum power of 100 W and a resonance frequency of 20 kHz was built. The strong and uniform sound field in the USMR was then applied to intensify gas–liquid mass transfer of slug flow in a microfluidic channel. Non-inertial cavitation with multiple surface wave oscillation was excited on the slug bubbles, enhancing the overall mass transfer coefficient by 3.3–5.7 times.

Introduction

Intensification of chemical and biological processes by ultrasound has a long history[1] and has become a popular area named sonochemistry since the early 1980s.[2–4] It was at about the same time that microfluidics emerged[5,6] and since then gained wide applications in biomedical analysis and chemical synthesis.[7–9] Until the beginning of this century ultrasound was gradually applied in microreactors,[10–14] which was recently recognized as a very promising area.[15–18] Due to its non-invasive nature[10–19] and strong acoustic effects like radiation force[20] and streaming,[21,22] ultrasound can be widely used to manipulate samples,[23–27] enhance mixing[28–31]/mass transfer[17,32] and prevent clogging in microreactors.[33,34] On the other hand, with a well-defined inner micro-structure, a microreactor provides an ideal environment to investigate and control the acoustic cavitation process,[15,35–40] which is the main mechanism for most power ultrasound applications.[41–43]

To introduce ultrasound into microfluidic channels, various types of USMR have been reported in the literature. In the early stage, microreactors integrated with piezoelectric films were used.[11–13,22] These devices need sophisticated micro-fabrication processes and lack generality in operation.[15] Currently, the most common USMR is composed of piezoelectric pieces directly glued to the outer surface of the microreactor[19–25] or compressed between the microreactor plates.[34] This kind of USMR is widely used in acoustophoresis[18,44] and acoustic bubble transducers,[23,27,30] since it is easy to fabricate and operate. However, as limited by low tensile strength and heat generation of the piezoelectric ceramic,[15] the power load of the piezoelectric piece is usually very low (from milliwatts to a few Watts), which limits its application in areas where high power is needed.

In the field of power ultrasound and sonochemistry, the Langevin-type ultrasonic transducer (LUT) is often used to generate high-power ultrasound.[45–47] The most convenient way to combine LUT and microreactor is directly immersing the microreactor in an ultrasonic cleaning bath.[32,48] But the water in the bath would also be cavitated, which dissipates a large portion of the input energy.[34] To overcome this issue, Hubner *et al.*[17] designed a vessel filled with pressured water (*ca.* 4.5 bar, the cavitation of the water was suppressed) to transmit the ultrasound from a LUT to the microreactor. This indirect energy input method has advantages of modularity and temperature control,[15,17,49] while the energy transfer efficiency is relatively low, due to the attenuation in the transmission medium and reflection at the liquid/solid interface. Directly coupling LUT with a microreactor is the most efficient way to deliver ultrasound into microreactors. For this type of USMR, the key is to design the structure of the LUT

[a] *Dalian National Laboratory for Clean Energy, Dalian Institute of Chemical Physics, Chinese Academy of Sciences, Dalian 116023, China. E-mail: gwchen@dicp.ac.cn*
[b] *University of Chinese Academy of Sciences, Beijing 100049, China*
[c] *Applied Acoustics Institute, Shaanxi Normal University, Xian, Shaanxi 710062, China*

† Electronic supplementary information (ESI) available. See DOI: 10.1039/c4lc01431f

and microreactor to ensure a robust, strong and uniform sound field in the microreactor. Tseng *et al.*[50] recently built a USMR by using a glass plate to connect the LUT and a PDMS microfluidic chip. The acoustic field was coupled into the microfluidic channel *via* the glass plate's flexural Lamb wave vibration, which is highly sensitive to the thickness and surface structure of the plate. So, the acoustic vibration pattern was altered and vibration amplitude was damped at the region where the PDMS chip is bonded.[50] In this paper, we present a novel high-power USMR with a microreactor plate directly coupled with LUT. The USMR is designed as a longitudinal half wavelength resonator, in which the antinode plane of the highest sound intensity is located at the microreactor plate. Compared to flexural vibration mode, such a longitudinal standing wave is more robust, energy efficient[45] and could achieve a quite uniform sound field in the microreactor.

The USMR was then used to intensify the gas–liquid mass transfer in a microfluidic channel. Many research results have shown that the mass transfer rate in microreactors is largely improved compared with conventional equipment.[51–54] As a result, many reactions can be operated in microreactors under much more harsh conditions to increase the reaction rate.[55] However, the improvement of mass transfer in microreactors is mainly due to the large specific surface area. The increase in mass transfer coefficient (k_L) is relatively not significant.[51–53] For some reactions of faster kinetics, the mass transfer needs to be further intensified.[55,56] As being able to create turbulence and streaming in the liquid, ultrasound has been used as an effective way in conventional equipment to enhance the gas–liquid mass transfer coefficient.[4,57–60] In this paper, the microreactor is combined with ultrasound to intensify gas–liquid mass transfer. Surface wave oscillation and microstreaming was excited on the slug bubbles, enhancing the overall mass transfer coefficient by 3.3–5.7 times.

Building the ultrasonic microreactor

Design of the USMR

LUT is composed of piezoelectric ceramic pieces clamped between the front mass and the back mass, which serve both to protect the piezoelectric ceramic and to prevent it from overheating by acting as a heat sink[45,46,61] (see the ESI†). When operated at resonance frequency, LUT vibrates as a half wavelength resonator[44] at the longitudinal direction, with the antinode plane located at the two ends. As the front mass is usually made of light metal and the back mass heavy metal, the vibration amplitude in the front surface of the transducer is the highest. If we directly couple the microreactor to the front surface of the LUT and let them vibrate as a similar longitudinal half wavelength resonator, the ultrasound would transmit into the microreactor efficiently, where the antinode plane with the highest and uniformly distributed ultrasound intensity is located (Fig. 1a).

To obtain this ideal state, the following aspects have to be emphasized when designing the USMR. 1) The structure of the microreactor needs to match the transducer to ensure pure longitudinal standing wave. The size of the microreactor in the longitudinal direction should be uniform, which means a flat plate is preferred. The size in the transverse direction should not be too much larger than the front surface of the LUT. Otherwise, flexural vibration mode of the microreactor will be excited and coupled with the longitudinal vibration, reducing the efficiency of the resonator.[45,61] 2) The sizes of each part of the USMR should be designed to keep the vibration node located at the piezoelectric pieces, in order to maximize the energy efficiency and lifespan of the piezoelectric element.[47] The node location and the resonance frequency can be predicted by one dimension design theory[45,61](see the ESI†), which can be used to guide the size design. 3) The coupling of the microreactor with the front mass should be rigid and without obvious transmission attenuation or reflection. Therefore, the microreactor and the front mass should be made of materials with similar acoustic impedance and coupled with a robust method.

Fabrication of the USMR

Considering our application, we designed and fabricated an USMR with a maximum power of 100 W and a resonance frequency of around 20 kHz (Fig. 1b). A commercial LUT (ZFHN-100-21.5, Baoding Zhengjie Electric, China) was purchased (see ESI† for more details). The aluminum alloy (LY12) front mass has a shape of a circular truncated cone, which could ensure a large radiation area (diameter of the front surface 66 mm). A square microreactor plate (made of LY12) with a length of 74 mm was used. Under the guidance of one dimension design theory, the thickness of the plate was chosen to be 3 mm, when the resonance frequency was calculated to be 20.38 kHz and the vibration node located at the upper piezoelectric piece (see the ESI† for the calculating details). The microreactor plate was then directly attached to the front surface of the LUT by an ultrasonic transmission gel (THD-383, Taiheda, China). To enhance the bonding strength, the two contact surfaces were sandblasted with corundum sand (36 mesh) at first. The connection was further reinforced by four long stainless steel screws (diameter 5 mm).

Characterization of the USMR

The vibration mode of this USMR was then checked by numerical simulation with ANSYS software. The vibration displacement distribution (Fig. 1c) showed that most part of the USMR is vibrating as a longitudinal half wavelength standing wave at its resonance state. The vibration node of lowest displacement locates in the piezoelectric pieces and the antinode of highest displacement in the microreactor. Only the four corners of the microreactor plate undergo flexural vibration, with the vibration amplitude first dropping near to zero and then rising to a high value near the four vertexes (see Fig. 1(d)). This dramatic vibration displacement variation is caused by the uneven excitation at the back of the microreactor, as the four corners are not covered by the transducer's front surface. Besides these corners, the vibration

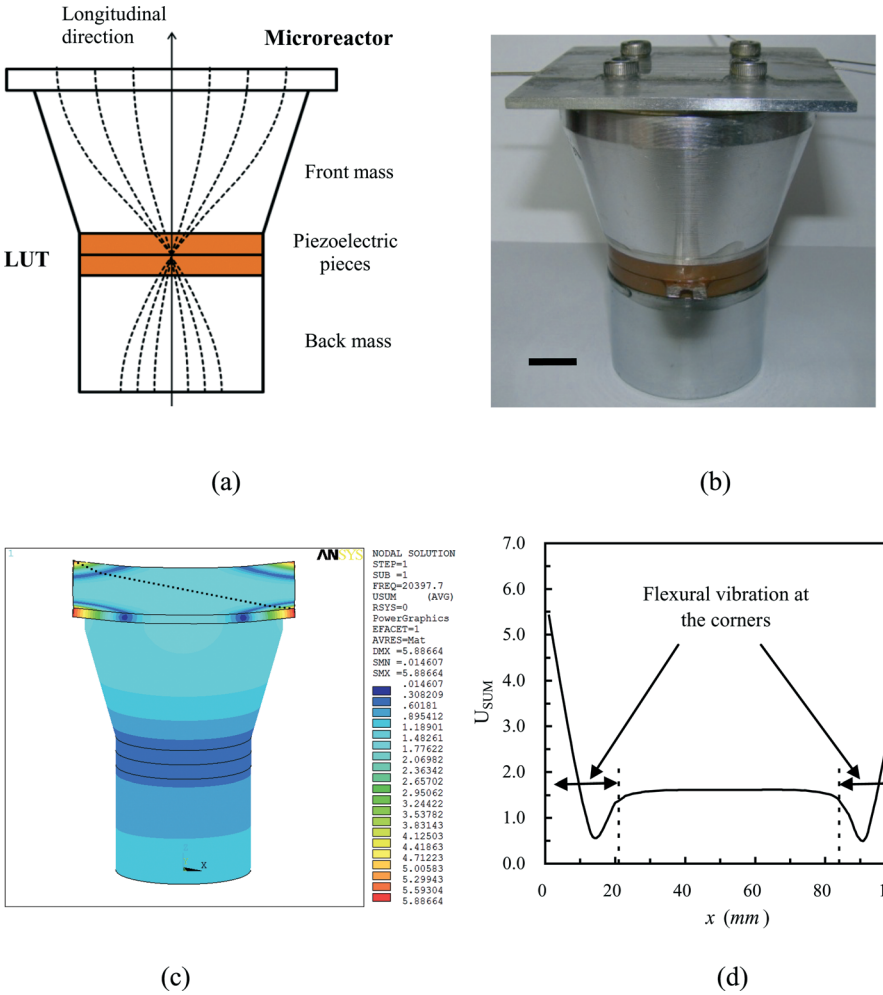

Fig. 1 (a) Design diagram of the ultrasonic microreactor. The dashed lines represent the half wavelength standing wave (or resonator). (b) Photo of the fabricated ultrasonic microreactor. The scale bar in the figure is 10 mm. (c) The simulated vibration displacement distribution of the ultrasonic microreactor at a resonance frequency of 20.4 kHz. (d) The simulated vibration displacement distribution (U_{SUM}) along the diagonal line on the surface of the microreactor (as indicated by the dashed line in Fig. 1(c)).

displacement amplitude in the center of the microreactor plate is almost the same, which means a quite uniform sound field (see Fig. 1(d)).

The resonance state of the USMR was also characterized using an impedance analyzer (PV70A, Beijing Band Era, China). No obvious flexural vibration peak was observed near the high longitudinal resonance peak in the measured admittance curves (Fig. 2). It indicates that the coupling of flexural vibration with longitudinal vibration is very weak and a pure longitudinal resonator is obtained. When the microreactor was coupled to the transducer, the resonance peak shifted from 21.66 kHz to 20.21 kHz, which was close to the theoretical value above. The measured resonance frequency, dynamic impedance and quality factor are displayed in Table 1. For a piezoelectric acoustic device, typically the lower is the dynamic impedance, the higher is the quality factor, which means higher electroacoustic transforming efficiency. As showed in Table 1, due to the loading of the microreactor, the dynamic impedance of the USMR increased while the quality factor decreased. During experimental operation, the

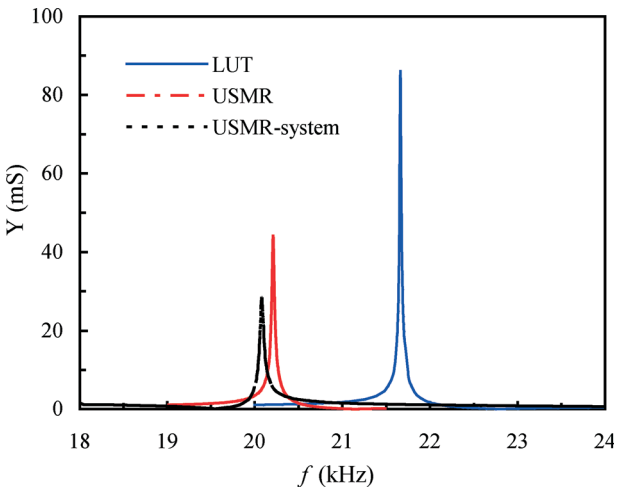

Fig. 2 Measured admittance (*Y*) of the LUT, USMR and USMR connected to system at different frequencies.

Table 1 The resonance frequency (f_R), dynamic impedance (R_1) and quality factor (Q_m) measured by the impedance analyzer

Parameter	LUT	USMR	USMR-system
f_R (kHz)	21.66	20.21	20.08
R_1 (Ω)	11.67	22.53	35.31
Q_m	1250.3	748.9	503.0

USMR needed to be sealed by a cover plate and connected to the inlet and outlet tubes, which would further increase the dynamic impedance and decrease the electroacoustic efficiency. To minimize these influences, the microreactor was sealed by a thin transparent polycarbonate film (0.2 mm in thickness) with epoxy glue, and connected with small stainless steel capillaries at the inlet and outlet (Fig. 1(b)). Even though those attempts were made, the resonance frequency of the USMR connected to the experiment system still shifted to 20.08 kHz and the quality factor decreased to 503.0 (Table 1).

Intensification of the gas–liquid mass transfer

Experimental setup

The efficiency of the USMR was then tested by a gas–liquid mass transfer process. The experimental system consisted of electrical, acoustic, flow and optical subsystems (Fig. 3(a)). In the electrical subsystem, the electrical signal generated by the ultrasonic generator (ZFDY-600FS, Baoding Zhengjie Electric, China) was used to drive the transducer. The effective input power and output wave form were recorded by a power meter and a digital oscilloscope (DS1052E, Rigol, China), respectively. In the acoustic subsystem, the electrical energy was converted into ultrasound wave by the LUT, which was then transmitted into the microchannels (see Fig. 3(b)) on the microreactor plate. A sponge bed at the bottom of the transducer was used to support the USMR and isolate the vibration. The ultrasound in the microchannel was then used

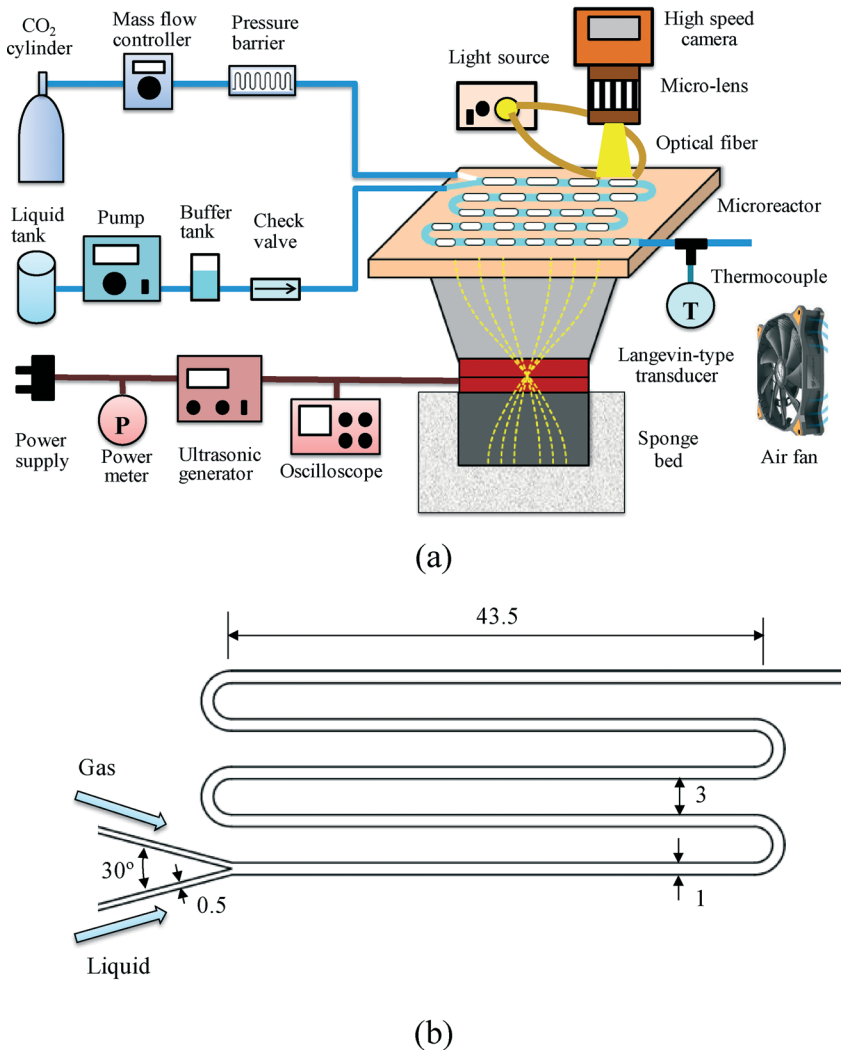

Fig. 3 (a) Schematic of the experimental setup. (b) The structure of the microchannel in the microreactor. The width of the inlet channels is 500 μm. The width of the main channel is 1 mm. The depth of all the channels is 1 mm.

to intensify the gas–liquid two phase flow, which was supplied by the flow subsystem. Physical absorption of pure CO_2 into deionized water was used. The mass transfer process was monitored by the optical subsystem. It consisted of a light source, two optical fibers for concentrated illumination, a macro lens and a high speed camera (Phantom M310, Vision Research, USA). Other details about the experimental setup can be found in the ESI.†

Before the mass transfer experiment, the actual working frequency of the system was first determined by sweeping the driving frequency of the ultrasonic generator around the designed resonance frequency. The frequency corresponding to the maximum input power was chosen as the working frequency. The value determined by this method was 19.70 kHz, which was then fixed in the following experiment. To alleviate the thermal effect of ultrasound, an air fan with a power of 20 W was put against the USMR to cool the system. Besides, to avoid a significant temperature rise, the ultrasonic generator was only turned on for a few minutes for each operating condition, during which the video of the gas–liquid two phase flow was recorded and then used for mass transfer measurement. When one experiment was completed, the ultrasonic generator was then turned off, while the air fan was still on to cool the system. The next experiment was conducted only when the temperature of the system was reduced to room temperature. The temperature rise in each operating condition was kept under 3 °C. The effect of this small temperature rise on the mass transfer measurement can be neglected at the present experiments, as was discussed in detail in the ESI.†

Slug bubble oscillation in USMR

Before turning on the ultrasonic generator, a stable gas–liquid slug flow (or Taylor flow)[62,63] was formed in the microfluidic channel. Due to the absorption of CO_2, the size of the gas bubbles decreased while moving downstream in the channel. When the ultrasound was exerted, the flowing slug bubbles oscillated vigorously (see the ESI†). The detail of the bubble oscillation was recorded by the high speed camera at a frame rate of 100 000 fps (see Video S1 in the ESI†). Since the electrical signal supplied to the LUT changed periodically (see the ESI†), the oscillation of the gas bubbles also had a periodical behavior.

As shown in Fig. 4 and Video S1,† the slug bubble's surface vibrated fiercely without collapsing, indicating that it undergoes non-inertial cavitation. Compared to the unsteady and transient inertial cavitation, bubble oscillation in non-inertial cavitation is more stable. It includes various oscillation modes depending on the acoustic pressure.[41,42,64] When the applied acoustic pressure is low, the bubble undergoes breathing oscillation mode with pulsation of the bubble volume. When the acoustic pressure exceeds a threshold, shape oscillation with many surface wave modes is excited. The surface wave mode with the lowest threshold is the Faraday wave mode, which appears as symmetrical peaks and valleys on the bubble surface. At higher acoustic pressure, many surface wave

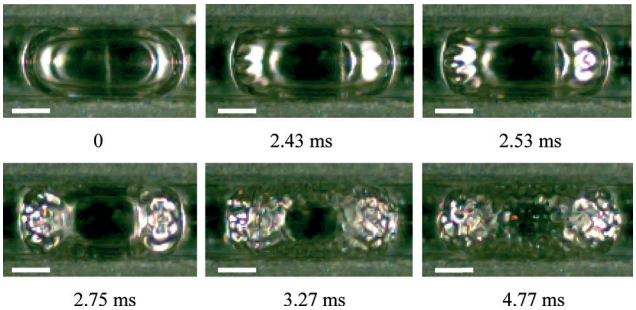

Fig. 4 Bubble oscillation at increasing ultrasound intensity from left to right. The six pictures were captured from Video S1† at different times, as indicated by the tags. As the input voltage increases with time at this period, the ultrasound intensity also increases with time. The scale bar in all the figures is 500 μm.

modes are superimposed, which leads to chaotic motion of the bubble surface.[15,65,66] The bubble in our experiment was confined by the microchannel and had a slug shape, but the cavitation behavior still corresponded to the above fact. As shown in Video S1† and Fig. 3, with the increase in the input electrical voltage, the bubble oscillation changed from volume pulsation to regular surface wave oscillation, and finally to chaotic surface distortion. Meanwhile, the area of significant surface distortion is increased. It started from the free bubble tips, and then gradually invaded the bubble waist confined by the microfluidic channel wall, and finally expanded to the entire bubble surface. It indicated that for a confined bubble surface, higher acoustic intensity was required to excite the surface wave modes than the free bubble surface.

Gas–liquid mass transfer intensification results

Due to the mass transfer of CO_2 from gas into water, the length of the slug bubbles decreases while moving downstream the channel. The faster is the mass transfer process, the higher is the decreasing rate of the bubble length. We have developed a unit cell model to analyse this mass transfer process.[67,68] An exponential type equation was obtained to describe the relationship between the bubble length and its location

$$L_B = m_1 + m_2 e^{-\frac{k_L a}{j_L} x} \quad (1)$$

where j_L is the superficial velocity of liquid. Parameters m_1 and m_2 depend only on the experimental conditions and the channel size. So, the overall volumetric mass transfer coefficient $k_L a$ can be determined by curve fitting the bubble length at different locations.

The bubble lengths at different locations in the channel were recorded and measured by a high speed camera. As shown in Fig. 5(a), without ultrasound irradiation, the bubble length decreases at a very slow rate. When ultrasound is introduced, the bubble length decreases faster and quickly approaches the equilibrium length when the water is almost saturated. Higher ultrasound intensity leads to a larger decreased rate of bubble length. The overall volumetric mass

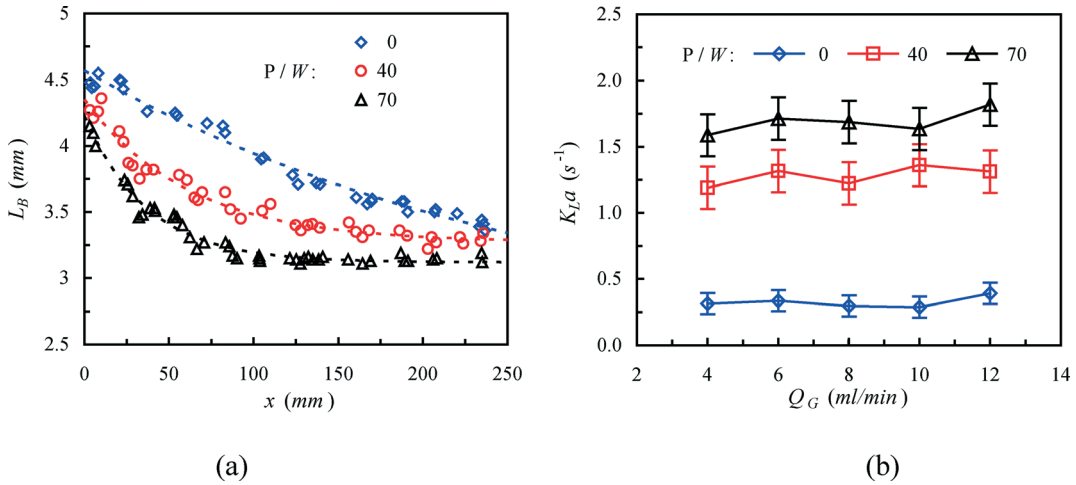

Fig. 5 (a) Lengths of a CO_2 slug bubble at different locations in the channel under different ultrasound power (Q_L = 4 ml min^{-1}, Q_G = 8 ml min^{-1}). The dashed lines are fitting curves according to eqn (1). (b) Mass transfer coefficient of the gas–liquid flow at a different gas flow rate with ultrasound power 0 W, 40 W and 70 W (Q_L = 4 ml min^{-1}). Each point was measured at least two times. For each power level, the maximum deviation was chosen for all points.

transfer coefficients were calculated by fitting the experimental data to eqn (1). As shown in Fig. 5(b), when ultrasound is not introduced, the overall volumetric mass transfer coefficient ranges from 0.29 to 0.39 s^{-1}, which is in consistent with results in the literature[69–71] for similar channel size and flow rates. With increasing gas flow rate, the mass transfer coefficient increases slightly, since larger bubble length is not beneficial for mass transfer. These phenomena have also been observed before.[51,67,72] Fig. 5(b) also shows that mass transfer can be greatly enhanced when ultrasound is present and mass transfer coefficient increases with increasing ultrasound power. In our experiments, the mass transfer coefficients range from 1.2 to 1.8 s^{-1}, which is about 3.3–5.7 times larger than those in the conditions without ultrasound. This significant mass transfer coefficient improvement is mainly caused by the fierce bubble oscillation phenomenon described in the last section. Surface wave oscillation of the slug bubble can dramatically increase the gas–liquid contact area. Besides, the fierce bubble oscillation could also create turbulence and streaming in the liquid near the interface, which further enhance the mass transfer coefficient. In fact, as a steady flow formed by the viscous dissipation of acoustic energy in the boundary layer of an oscillating bubble, cavitation microstreaming always appears with surface wave oscillation.[15,21,31,41,73] It has been widely used to pump fluid[30,74] and enhance mixing.[19,21,27,29,31,40] It can be expected that this kind of microstreaming is also present near the oscillating slug bubbles in our experiment, which would significantly accelerate the gas–liquid mass transfer process.

This enhancement of mass transfer coefficient in our USMR is much higher than that in conventional ultrasonic reactors, which is usually between 10% and 110%.[4,57,59,60] There are two possible reasons. Firstly, the ultrasound power density in our USMR (0.13–1.4 W ml^{-1}, see the ESI† for more details) is higher than that in conventional reactors (usually between 0.05–0.6 W ml^{-1}), due to the relatively small volume of the microreactor and high energy efficiency of the USMR design. Secondly, the intensification mechanism in our USMR—non-inertial cavitation with fierce surface wave oscillation and microstreaming—is more stable and uniformly distributed than in conventional reactors. As the sound field in the microreactor plate is quite uniform, all the bubbles in the microreactor are in fierce oscillation (see Fig. S3(b) in the ESI†), which is difficult to achieve in conventional large ultrasonic reactors.[4,16,58,59]

Conclusion

A robust USMR vibrating as a half wavelength resonator was designed and fabricated, according to one dimension design theory, numerical simulation and impedance analysis. A strong and uniform sound field is generated in the microreactor. As the USMR is built by directly coupling a microreactor plate to a commercial available LUT (~US$15), the fabrication process is relatively simple and low cost. The design concept and method can be used to fabricate USMR with higher power, larger volume and higher throughput. The gas–liquid mass transfer was significantly enhanced in our USMR, due to the high ultrasound power density, stable and uniformly distributed intensification mechanism—fierce surface wave oscillation of the slug bubble. If the electronic subsystem (especially the wave form of the ultrasonic generator) is further optimized, the mass transfer enhancement would be larger. This USMR can be an efficient and versatile tool for the microfluidic communities, which could be applied to intensify mixing and chemical reactions, prevent clogging, handle biomaterials, study acoustic cavitation processes and so on.

Acknowledgements

We acknowledge the financial support for this project from the National Natural Science Foundation of China (no.

21225627 and 91334201) and the Ministry of Science and Technology of China (no. 2012BAA08B02). Authors would like to thank Jiansheng Chu, Hengqiang Li and Fengjun Jiao (Dalian Institute of Chemical Physics) for their help in manufacturing the microreactor and building the experimental setup.

References

1 R. W. Wood and A. L. Loomis, *Philos. Mag.*, 1927, **4**, 414–436.
2 K. S. Suslick, *Ultrasound: its chemical, physical, and biological effects*, VCH Publishers, 1988.
3 A. Stankiewicz, *Chem. Eng. Res. Des.*, 2006, **84**, 511–521.
4 P. R. Gogate, V. S. Sutkar and A. B. Pandit, *Chem. Eng. J.*, 2011, **166**, 1066–1082.
5 S. C. Terry, J. H. Jerman and J. B. Angell, *IEEE Trans. Electron Devices*, 1979, **26**, 1880–1886.
6 D. B. Tuckerman and R. F. W. Pease, *IEEE Electron Device Lett.*, 1981, **2**, 126–129.
7 K. Jahnisch, V. Hessel, H. Löwe and M. Baerns, *Angew. Chem., Int. Ed.*, 2004, **43**, 406–446.
8 G. M. Whitesides, *Nature*, 2006, **442**, 368–373.
9 R. L. Hartman and K. F. Jensen, *Lab Chip*, 2009, **9**, 2495–2507.
10 K. Yasuda, *Sens. Actuators, B*, 2000, **64**, 128–135.
11 Z. Yang, S. Matsumoto, H. Goto, M. Matsumoto and R. Maeda, *Sens. Actuators, A*, 2001, **93**, 266–272.
12 J. C. Rife, J. S. Horwitz, M. I. Bell, M. N. Kabler, R. C. Y. Auyeung and W. J. Kim, *Sens. Actuators, A*, 2000, **86**, 135–140.
13 G. G. Yaralioglu, I. O. Wygant, T. C. Marentis and B. T. Khuri-Yakub, *Anal. Chem.*, 2004, **76**, 3694–3698.
14 M. Bengtsson and T. Laurell, *Anal. Bioanal. Chem.*, 2004, **378**, 1716–1721.
15 Y. Iida, T. Tuziuti, K. Yasui, A. Towata and T. Kozuka, *Ultrason. Sonochem.*, 2007, **14**, 621–626.
16 D. F. Rivas, P. C. Cintas and H. J. G. E. Gardeniers, *Chem. Commun.*, 2012, **48**, 10935–10947.
17 S. Hubner, S. Kressirer, D. Kralisch, C. Bludszuweit-Philipp, K. Lukow, I. Janich, A. Schilling, H. Hieronymus, C. Liebner and K. Jahnisch, *ChemSusChem*, 2012, **5**, 279–288.
18 H. Bruus, J. Dual, J. Hawkes, M. Hill, T. Laurell, J. Nilsson, S. Radel, S. Sadhal and M. Wiklund, *Lab Chip*, 2011, **11**, 3579–3580.
19 D. Ahmed, X. Mao, B. K. Juluri and T. J. Huang, *Microfluid. Nanofluid.*, 2009, **7**, 727–731.
20 L. A. Kuznetsova and W. T. Coakley, *Biosens. Bioelectron.*, 2007, **22**, 1567–1577.
21 M. Wiklund, R. Green and M. Ohlin, *Lab Chip*, 2012, **12**, 2438–2451.
22 L. Johansson, S. Johansson, F. Nikolajeff and S. Thorslun, *Lab Chip*, 2009, **9**, 297–304.
23 M. V. Patel, A. R. Tovar and A. P. Lee, *Lab Chip*, 2012, **12**, 139–145.
24 P. Marmottant and S. Hilgenfeldt, *Proc. Natl. Acad. Sci. U. S. A.*, 2004, **101**, 9523–9527.
25 C. Wang, S. V. Jalikop and S. Hilgenfeldt, *Biomicrofluidics*, 2012, **6**, 012801.
26 D. Rabaud, P. Thibault, M. Mathieu and P. Marmottant, *Phys. Rev. Lett.*, 2011, **106**, 134501.
27 A. Hashmi, G. Yu, M. Reilly-Collette, G. Heiman and J. Xu, *Lab Chip*, 2012, **12**, 4216–4227.
28 R. H. Liu, J. Yang, M. Z. Pindera, M. Athavale and P. Grodzinski, *Lab Chip*, 2002, **2**, 151–157.
29 D. Ahmed, X. Mao, J. Shi, B. K. Juluri and T. J. Huang, *Lab Chip*, 2009, **9**, 2738–2741.
30 A. R. Tovar and A. P. Lee, *Lab Chip*, 2009, **9**, 41–43.
31 C. Wang, B. Rallabandi and S. Hilgenfeldt, *Phys. Fluids*, 2013, **25**, 022002.
32 S. Aljbour, T. Tagawa and H. Yamada, *J. Ind. Eng. Chem.*, 2009, **15**, 829–834.
33 R. L. Hartman, J. R. Naber, N. Zaborenko, S. L. Buchwald and K. F. Jensen, *Org. Process Res. Dev.*, 2010, **14**, 1347–1357.
34 S. Kuhn, T. Noel, L. Gu, P. L. Heider and K. F. Jensen, *Lab Chip*, 2011, **11**, 2488–2492.
35 A. Stankiewicz, *Ind. Eng. Chem. Res.*, 2007, **46**, 4232–4235.
36 Y. Iida, K. Yasui, T. Tuziuti, M. Sivakumar and Y. Endo, *Chem. Commun.*, 2004, 2280–2281.
37 D. F. Rivas, M. Ashokkumar, T. Leong, K. Yasui, T. Tuziuti, S. Kentish, D. Lohse and H. J. G. E. Gardeniers, *Ultrason. Sonochem.*, 2012, **19**, 1252–1259.
38 T. Tandiono, S. W. Ohl, D. S. W. Ow, E. Klaseboer, V. V. Wong, R. Dumkec and C. D. Ohl, *Proc. Natl. Acad. Sci. U. S. A.*, 2011, **108**, 5996–5998.
39 T. Tandiono, S. W. Ohl, D. S. W. Ow, E. Klaseboer, V. V. Wong, A. Camattari and C. D. Ohl, *Lab Chip*, 2010, **10**, 1848–1855.
40 A. Ozcelik, D. Ahmed, Y. Xie, N. Nama, Z. Qu, A. A. Nawaz and T. J. Huang, *Anal. Chem.*, 2014, **86**, 5083–5088.
41 T. G. Leighton, *The Acoustic Bubble*, Academic Press Limited, London, 1994.
42 T. G. Leighton, *Prog. Biophys. Mol. Biol.*, 2007, **93**, 3–83.
43 J. Rooze, E. V. Rebrov, J. C. Schouten and J. T. F. Keurentjes, *Ultrason. Sonochem.*, 2013, **20**, 1–11.
44 A. Lenshof, M. Evander, T. Laurell and J. Nilsson, *Lab Chip*, 2012, **12**, 684–695.
45 S. Lin, *The mechanism and design of ultrasound transducer*, Science Press, Beijing, 2004, (in Chinese).
46 T. J. Mason and D. Peters, *Applied Sonochemistry: Uses of Power Ultrasound in Chemistry and Processing*, Wiley-VCH, 2002.
47 A. Mathieson, A. Cardoni, N. Cerisola and M. Lucas, *IEEE Trans. Ultrason., Ferroelectr., Freq. Control*, 2013, **60**, 1126–1133.
48 T. Horie, M. Sumino, T. Tanaka, Y. Matsushita, T. Ichimura and J. Yoshida, *Org. Process Res. Dev.*, 2010, **14**, 405–410.
49 R. Dominique, R. Fabio, Q. Wilhelm, G. Michael and E. Markus, *WO Pat.*, 2011 023761 A1, 2011.
50 Q. Tseng, A. M. Lomonosov, E. E. M. Furlong and C. A. Merten, *Lab Chip*, 2012, **12**, 4677–4682.
51 J. Yue, G. W. Chen, Q. Yuan, L. Luo and Y. Gonthier, *Chem. Eng. Sci.*, 2007, **62**, 2096–2108.

52 P. Sobieszuk, J. Aubin and R. Pohorecki, *Chem. Eng. Technol.*, 2012, **35**, 1346–1358.
53 M. J. Nieves-Remacha, A. A. Kulkarni and K. F. Jensen, *Ind. Eng. Chem. Res.*, 2013, **52**, 8996–9010.
54 M. N. Kashid, A. Renken and L. Kiwi-Minsker, *Chem. Eng. Sci.*, 2011, **66**, 3876–3897.
55 V. Hessel, D. Kralisch, N. Kockmann, T. Noel and Q. Wang, *ChemSusChem*, 2013, **6**, 746–789.
56 N. Kockmann, *Transport phenomena in micro process engineering: Fundamentals, devices, fabrication, and applications*, Springer, Berlin, 2008.
57 M. L. Cadwell and H. S. Fogler, *Chem. Eng. Prog., Symp. Ser.*, 1971, **67**, 124–127.
58 N. S. Herran, J. L. Casas Lopez and J. A. S. Pere, *Ind. Eng. Chem. Res.*, 2012, **51**, 2769–2774.
59 A. Kumar, P. R. Gogate, A. B. Pandit, H. Delmas and A. M. Wilhelm, *Ind. Eng. Chem. Res.*, 2004, **43**, 1812–1819.
60 N. Gondrexon, V. Renaudin, P. Boldo, Y. Gonthier, A. Bernis and C. Petrier, *Chem. Eng. J.*, 1997, **66**, 16–21.
61 M. D. McCollum, B. F. Hamonic and O. B. Wilson, *Transducers for Sonics and Ultrasonics*, Technomic, Lancaster, PA, 1993.
62 Y. C. Zhao, G. W. Chen, C. B. Ye and Q. Yuan, *Chem. Eng. Sci.*, 2013, **87**, 122–132.
63 C. Q. Yao, Y. C. Zhao, C. B. Ye, M. H. Dang, Z. Y. Dong and G. W. Chen, *Chem. Eng. Sci.*, 2013, **95**, 246–256.
64 P. R. Birkin, D. G. Offin, C. J. Vian, T. G. Leighton and A. O. Maksimov, *J. Acoust. Soc. Am.*, 2011, **130**, 3297–3308.
65 D. G. Offin, P. R. Birkin and T. G. Leighton, *Electrochem. Commun.*, 2007, **9**, 1062–1068.
66 P. R. Birkin, Y. E. Watson and T. G. Leighton, *Chem. Commun.*, 2001, 2650–2651.
67 C. Q. Yao, Z. Y. Dong, Y. C. Zhao and G. W. Chen, *Chem. Eng. Sci.*, 2014, **112**, 15–24.
68 C. Q. Yao, Z. Y. Dong, Y. C. Zhao and G. W. Chen, *Chem. Eng. Sci.*, 2015, **123**, 137–145.
69 C. O. Vandu, H. Liu and R. Krishna, *Chem. Eng. Sci.*, 2005, **60**, 6430–6437.
70 J. M. van Baten and R. Krishna, *Chem. Eng. Sci.*, 2004, **59**, 2535–2545.
71 J. Yue, L. Luo, Y. Gonthier, G. W. Chen and Q. Yuan, *Chem. Eng. Sci.*, 2009, **64**, 3697–3708.
72 J. Tan, Y. C. Lu, J. H. Xu and G. S. Luo, *Chem. Eng. J.*, 2012, **181**, 229–235.
73 S. A. Elder, *J. Acoust. Soc. Am.*, 1959, **31**, 54–64.
74 K. Ryu, S. K. Chung and S. K. Cho, *J. Lab. Autom.*, 2010, **15**, 163–171.

